Impact of Data Assimilation on ECCO2 Equatorial Undercurrent and North Equatorial Countercurrent in the Pacific Ocean

DAVID HALPERN AND DIMITRIS MENEMENLIS

Jet Propulsion Laboratory, California Institute of Technology, Pasadena, California

XIAOCHUN WANG

University of California, Los Angeles, Los Angeles, California

(Manuscript received 4 February 2014, in final form 4 September 2014)

ABSTRACT

The impact of data assimilation on the transports of eastward-flowing Equatorial Undercurrent (EUC) and North Equatorial Countercurrent (NECC) in the Pacific Ocean from 145°E to 95°W during 2004–05 and 2009–11 was assessed. Two Estimating the Circulation and Climate of the Ocean, Phase II (ECCO2), solutions were analyzed: one with data assimilation and one without. Assimilated data included satellite observations of sea surface temperature and ocean surface topography, in which the sampling patterns were approximately uniform over the 5 years, and in situ measurements of subsurface salinity and temperature profiles, in which the sampling patterns varied considerably in space and time throughout the 5 years. Velocity measurements were not assimilated. The impact of data assimilation was considered significant when the difference between the transports computed with and without data assimilation was greater than $5.5 \times 10^6\,m^3\,s^{-1}$ (or 5.5 Sv; $1\,Sv \equiv 10^6\,m^3\,s^{-1}$) for the EUC and greater than 5.0 Sv for the NECC. In addition, the difference of annual-mean transports computed from 3-day-averaged data was statistically significant at the 95% level. The impact of data assimilation ranged from no impact to very substantial impact when data assimilation increased the EUC transport and decreased the NECC transport. The study's EUC results had some correspondence with other studies and no simple agreement or disagreement pattern emerged among all studies of the impact of data assimilation. No comparable study of the impact of data assimilation on the NECC has been made.

1 Introduction

The Equatorial Undercurrent (EUC) and North Equatorial Countercurrent (NECC) are major tropical ocean currents that transport warm water eastward in the uppermost 300–400 m. The EUC and NECC occur at the equator and 7.5°N, respectively, with latitudinal widths of 3° and 5°, respectively. The EUC and NECC are maintained by zonal wind stress and wind stress curl, respectively. In the Pacific Ocean, the EUC is strongly related to the onset, maintenance, and dissipation of the El Niño/La Niña phenomenon and the NECC is coupled to the intertropical convergence zone (Philander 1990). Studies of the importance of EUC horizontal and vertical advections of heat (Bindoff et al. 2007), chlorophyll-*a* (Martin et al. 1994), carbon dioxide (Takahashi et al. 2009), and other properties have been limited by the virtual absence of upper-ocean current measurements.

Sustained upper-ocean current measurements in the EUC occur at five sites (McPhaden et al. 1998), where the EUC core depth varies from 225 m to 75 m. No such in situ current measurements occur in the NECC. In contrast to the very small number of direct current observations, currents generated with an ocean general circulation model (OGCM) constrained by observations provide an exceedingly large number of virtual current meters, which invites exploration of their utility in studies of ocean circulation. The tenet of faith that an OGCM constrained by observations would yield a significantly different representation of upper-ocean currents will be tested in this paper.

Many OGCMs and ocean data assimilation systems are available (e.g., Balmaseda et al. 2013; Vernieres et al. 2012;

Corresponding author address: David Halpern, Jet Propulsion Laboratory, California Institute of Technology, M/S 233-300, 4800 Oak Grove Dr., Pasadena, CA 91109.
E-mail: david.halpern@jpl.nasa.gov

DOI: 10.1175/JTECH-D-14-00025.1

Carton et al. 2000). This study examines numerical solutions of the horizontal velocity field produced by the Estimating the Circulation and Climate of the Ocean, Phase II (ECCO2), project (Menemenlis et al. 2008). We chose ECCO2 solutions because their 19.6-km horizontal grid spacing is sufficient to resolve low-latitude eddy motions (Hallberg 2013) and the EUC and NECC north–south boundaries. ECCO2 solutions are obtained by fitting a global, full-depth ocean and sea ice configuration of the Massachusetts Institute of Technology general circulation model (MITgcm) to satellite and in situ observations using the adjoint method (Wunsch and Heimbach 2007; Wunsch et al. 2009). The adjoint method permits solutions that minimize a weighted quadratic difference between OGCM and observations while satisfying OGCM conservation laws of heat, salinity, and momentum for the complete assimilation period. In particular, ECCO2 solutions do not contain discontinuities when and where data are ingested. State estimation is very different from meteorological data assimilation because the latter does not conserve energy, freshwater, or heat, and is dynamically inconsistent with gravity wave shocks produced at each assimilation period. ECCO2 solutions generated without and with data assimilation are referred to as Baseline and Optimized, respectively.

We did not know a priori whether ECCO2 Optimized solutions would produce higher, lower, or unchanged EUC transport compared to the Baseline. And, we did not know a priori whether the NECC transport would increase, decrease, or remain unchanged with data assimilation. In situ current measurements recorded at the equator, which had not been used in the assimilation procedure, were used to demonstrate that ECCO2 Optimized solutions represented, to a high degree, in situ current observations. No in situ current measurements existed in the NECC.

2. Methods

The ECCO2 configuration of the MITgcm has 12 equal vertical layers from the surface to 120 m, 10 additional layers of varying thicknesses over the next 324 m, and up to 28 layers extending to the ocean bottom when the depth is greater than 6 km. The EUC and NECC are confined to the uppermost 400 m. The model integration time step was 20 min and the 3-day-averaged output was archived. ECCO2 solutions were available for two time intervals, 2004–05 and 2009–11, that had been developed for different research objectives. Although the 2004–05 and 2009–11 solutions were produced independently, all OGCM parameters, such as horizontal and vertical mixing coefficients, were the same in both time intervals and were obtained using a Green's function approach (Menemenlis et al. 2005). Near-surface vertical mixing in the tropics follows Large et al. (1994) with a background viscosity of $5.7 \times 10^{-4}\,\mathrm{m^2\,s^{-1}}$ and a diffusivity of $4.4 \times 10^{-6}\,\mathrm{m^2\,s^{-1}}$. There is no explicit horizontal diffusivity but a third-order direct space–time advection scheme is used, which adds sufficient diffusion for stability. Grid-size-dependent biharmonic horizontal viscosity is applied with values ranging from 1.25×10^{11} to $2.5 \times 10^{11}\,\mathrm{m^4\,s^{-1}}$ in the tropics.

Initial conditions for the Baseline 2004–05 simulation were obtained from a 2-yr spinup of the OGCM from rest with Forget (2010) mean temperature and salinity distributions. Initial conditions for the Baseline 2009–11 simulation were the end state of the Optimized 2004–05 solution. The 2004 and 2009 initial conditions were then modified, along with surface boundary conditions, by the adjoint method optimization (Wunsch and Heimbach 2007). The initial conditions influence the mean stratification and magnitudes of EUC and NECC, but they have little impact on transport variations. In the adjoint method, a scalar cost function, which measures the quadratic distance between observations and the simulation is minimized iteratively. During each iteration we first integrate the model forward, then we use the adjoint model to linearize the OGCM and compute gradients of the scalar cost function relative to the "control" parameters; finally, we adjust the control parameters in a direction that reduces the cost function. In addition to the initial temperature and salinity conditions, the control parameters include surface wind and other atmospheric boundary conditions. In particular, wind stress and its curl are modified by the data assimilation. Because the OGCM is nonlinear, several such forward-adjoint iterations are needed to reach a solution that is statistically consistent with model and data error estimates.

Table 1 lists assimilated datasets and prescribed errors in the cost function, which differ for 2004–05 and 2009–11. The European Centre for Medium-Range Weather Forecasts (ECMWF) operational analysis and the Japan Meteorological Agency (JMA) reanalysis of surface atmospheric variables were used as first-guess surface atmospheric boundary conditions for the 2004–05 and 2009–11 solutions, respectively. ECMWF and JMA atmospheric fields were also included in the 2004–05 and 2009–11 cost functions, respectively. Because the OGCM is nonlinear, the first-guess wind products will lead to different wind stress estimates, even if all terms in the cost function were identical. Jason sea level anomaly (SLA) measurements were assimilated in all years but *Environmental Satellite* (*Envisat*) SLA data were assimilated only in 2004–05. Sea surface temperature (SST) observations had essentially the same sampling characteristics

TABLE 1. Assimilated datasets and prescribed errors in 2004–05 and 2009–11. Ocean surface temperatures were provided by the Advanced Microwave Scanning Radiometer for Earth Observing System (AMSR-E) instrument on the NASA satellite *Aqua* from 1 Jan 2009 to 4 Oct 2011 and by the WindSat instrument on the U.S. Navy *Coriolis* satellite from 5 Oct to 31 Dec 2011. Arctic Ocean sea ice data are not shown.

Assimilated dataset	2004–05	2009–11
Surface atmosphere (model analyses)	ECMWF operational analysis	JMA reanalysis
Prescribed errors	Variance of fields	
Temp profiles (in situ)	XBT	No XBT data assimilated
Prescribed errors	Forget and Wunsch (2007)	
Temp and salinity profiles (in situ)	Argo	Argo
Prescribed errors	Forget and Wunsch (2007)	
Temp and salinity atlas	Forget (2010)	Forget (2010)
Prescribed errors	Variance of model-data difference	
SLA (satellite)	*Jason-1* + Envisat	*Jason-2*
Prescribed errors	Variance of model-data difference	
	~25 cm^2	~25 cm^2
SST (satellite)	AMSR-E	AMSR-E/WindSat
Prescribed errors	Variance of model-data difference	
	0.3°–1.3°C	0.5°C

in 2004–05 and 2009–11, but the prescribed errors differed (Table 1). The geographical and temporal distributions of in situ salinity and temperature profiles varied greatly (Fig. 1). Expendable bathythermograph (XBT) temperature profiles in 2009–11 and the Tropical Atmosphere Ocean (TAO) moored-buoy temperature profiles in 2004–05 and 2009–11 were inadvertently omitted from data assimilation. The absence of TAO data, unfortunately, represents the recent degraded state of the TAO array (Tollefson 2014). Argo temperature and salinity profile measurements were assimilated in all years and, as the Argo program matured, the quantity and geographical coverage increased each year (Fig. 1). The minimum amount of in situ data available for assimilation in the EUC and NECC regions occurred in 2004. Only slightly more in situ data were assimilated in 2010 compared to 2004. The geographical coverage and quantity of temperature and salinity profiles assimilated in the EUC and NECC regions were greatest in 2011. No estimate was made of the minimum amount of in situ data required for a reliable description of the equatorial currents' variability because a lack of resources prevented ECCO2 data selection experiments, in which certain datasets are excluded from the assimilation scheme to determine ECCO2 solutions.

The cost function included quadratic model-data differences for all the above-mentioned datasets with the following prescribed error variances (Table 1). For ECMWF and JMA fields, we used their full variance. Prescribed SLA error was the variance of the model-data difference, which was approximately 25 cm^2 in the equatorial Pacific. In 2004–05 the prescribed SST error was the variance of the model-data difference ranging from 0.3°C^2 in the western equatorial Pacific to 1.3°C^2 in the eastern equatorial Pacific; in 2009–11, the prescribed SST error variance was 0.5°C^2. Prescribed errors for all in situ temperature and salinity profile observations were from Forget and Wunsch (2007). In addition the cost function included a climatological constraint to the Forget (2010) temperature and salinity atlas with prescribed error as the variance of the model-data difference. The SLA prescribed error did not include any off-diagonal terms.

3 Results

a. Comparison with in situ measurements

Annual cycles of the EUC and NECC transports were measured only once, and that was in 1979–80 (Wyrtki and Kilonsky 1984), which occurred before the development of ECCO. However, the National Oceanic and Atmospheric Administration (NOAA) has sustained moored upper-ocean acoustic Doppler current profiler (ADCP) measurements at several sites along the Pacific equator. Therefore, to provide a sense of the accuracy of ECCO2 solutions of the EUC transports, the ECCO2 Optimized and ADCP eastward transport per unit width at the equator were compared at 140° and 110°W, where the two longest ADCP measurements occurred during the ECCO2 years. Minor data gaps were filled through linear interpolation. No similar comparison of the eastward

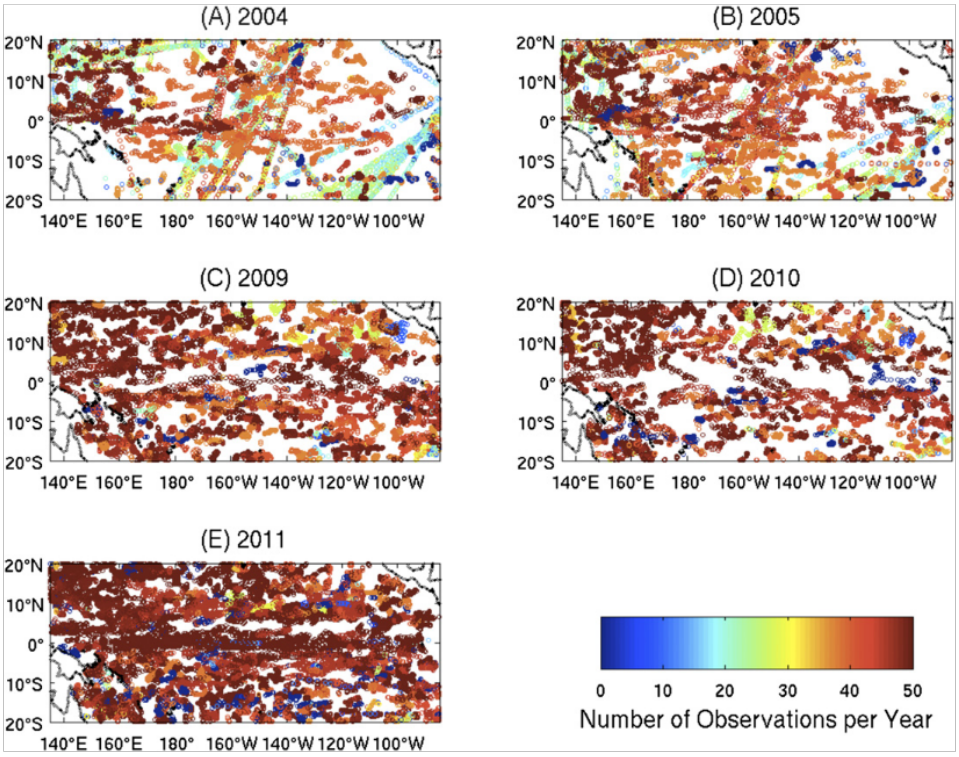

FIG. 1. Distributions of XBT temperature profiles and Argo temperature and salinity profiles in (a) 2004 and (b) 2005. Distributions of Argo temperature and salinity profiles in (c) 2009, (d) 2010, and (e) 2011.

transport per unit width was made within the NECC because in situ current measurements did not exist during ECCO2 years, or in other years.

The eastward transport per unit width was equal to $\int u(>0)\,dz$, where $u(>0)$ was the eastward component of the zonal current; no westward flow was considered. An arbitrary depth interval, dz, of 35–195 m was chosen because it was a common interval for ADCP measurements in the Atlantic, Indian, and Pacific Oceans during ECCO2 years. The 1-day-averaged ADCP observations, which were obtained from online (http://www.pmel.noaa.gov/tao/jsdisplay/), were bin averaged over 3 days to conform to the 3-day-averaged ECCO2 Optimized solutions.

The ADCP and ECCO2 Optimized eastward transport per unit width time series at 140° and 110°W are shown in Fig. 2. At both sites, the mean ADCP values were larger than ECCO2 solutions, with record-length mean biases of 30 and 12 $m^2 s^{-1}$ at 140° and 110°W, respectively. The variability of 3-day values, as represented by the standard deviation, was larger by about 40% in the ADCP measurements compared to ECCO2 solutions, which can be caused by processes that are not explicitly represented in the model, for example, short-period and tidal internal gravity wave motions and insufficient variability in the atmospheric forcing fields. The 95% statistically significant correlation coefficients were 0.83 and 0.78 at 140° and 110°W, respectively, which are indications that ECCO2 captured the main characteristics of variability of ADCP time series. For monthly-mean values, the correlation coefficients at 140° and 110°W were 0.89 and 0.76, respectively. The correlation coefficients for 3-day and monthly data were 95% statistically higher at 140° than at 110°W, which, perhaps, was a result of the stronger EUC current at 140° than at 110°W in the presence of ubiquitous Kelvin and tropical instability waves. Regression analysis of the 3-day data shown in Fig. 2 had least squares lines of ECCO2 ($m^2 s^{-1}$) = 0.68 ADCP ($m^2 s^{-1}$) + 10.4 $m^2 s^{-1}$ at 140°W and ECCO2 ($m^2 s^{-1}$) = 0.55 ADCP ($m^2 s^{-1}$) + 35.0 $m^2 s^{-1}$ at 110°W. The 3-day ECCO2 values were higher (smaller) than ADCP measurements when ADCP values were smaller (higher) than 32.3 and 77.8 $m^2 s^{-1}$ at 140° and 110°W, respectively. It is tempting to speculate that the dissimilarity of the slopes of the regression curve at 140° and 110°W was caused by lower ADCP noise levels (e.g., mooring motions) associated with a stronger EUC, which occurred at 140° compared to

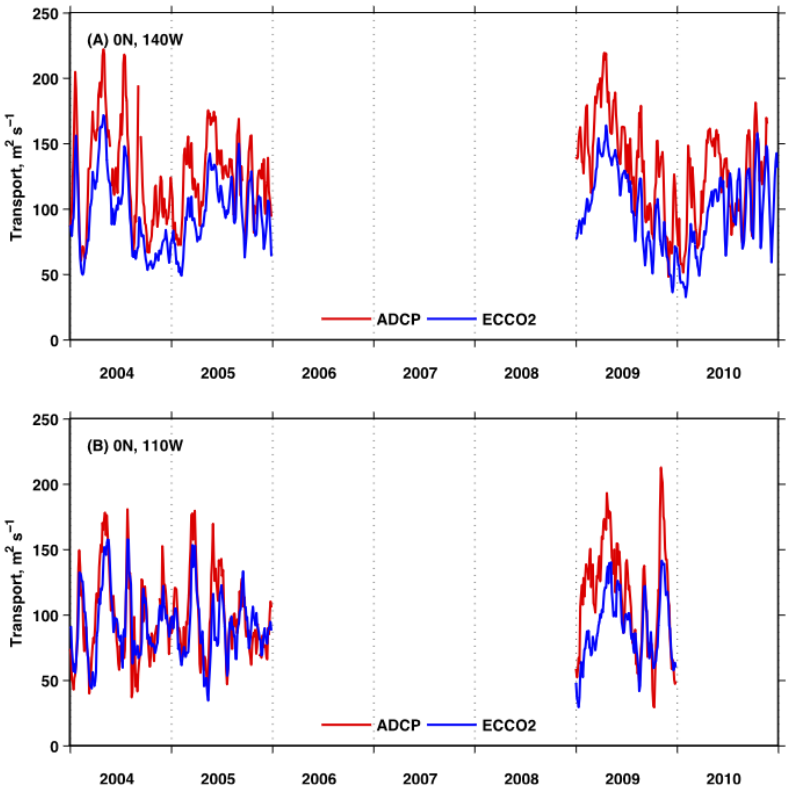

FIG. 2. Time series of 3-day-averaged ADCP and ECCO2 Optimized eastward transport per unit width between 35 and 195 m at (a) 0°, 140°W and (b) 0°, 110°W.

110°W (Fig. 2). Root-mean-square (RMS) differences at 140° and 110°W were 36.4 and 26.0 $m^2 s^{-1}$, respectively, indicating opportunities to improve the representativeness of ECCO2 solutions.

The ADCP magnitude of the crest of fluctuations was much larger than that produced by ECCO2, while ADCP and ECCO2 representations of fluctuation troughs were similar (Fig. 2), which produced larger ADCP mean and standard deviation values. This feature was more pronounced at 140° than 110°W. Each year the two-site average ADCP means and standard deviations were greater by an average of 22% and 33%, respectively, than those computed with the ECCO2 Optimized solution. The larger ADCP variability occurred at intraseasonal and annual time scales, and varied from year to year and between the two sites. In 2004, the annual means at 110°W differed by 2%, whereas the annual means at 140°W in 2004 and 2009 differed by 36%. Intraseasonal fluctuations, which were represented by a succession of Kelvin wave pulses (Halpern et al. 2013) and, presumably, tropical instability wave motion, and the annual cycle were clearly occurring concurrently in both datasets. ADCP periodogram ordinates (spectral energy with 2 degrees of freedom) were higher at nearly all frequencies (not shown) compared to those computed with ECCO2 solutions, although ADCP and ECCO2 differences were not statistically significant at 95% confidence level.

The intercomparison test of the eastward transport per unit width at the equator showed that ECCO2 Optimized solutions and moored ADCP measurements had similar attributes. Considering the very different spatial and temporal characteristics of the two datasets, in which ADCP measurements represented ocean motions at a virtual point compared to the wide spatial domain of the ECCO2 Optimized solutions, the correspondence between ADCP and ECCO2 datasets was deemed very good. We note that the EUC transport per unit width was strongly correlated with the EUC volume transport with a correlation coefficient of 0.99 (Knox and Halpern 1982).

b. *Time-averaged currents*

To provide a first-order representation of the EUC and NECC, the 5-yr-averaged (2004–05, 2009–11) north–south

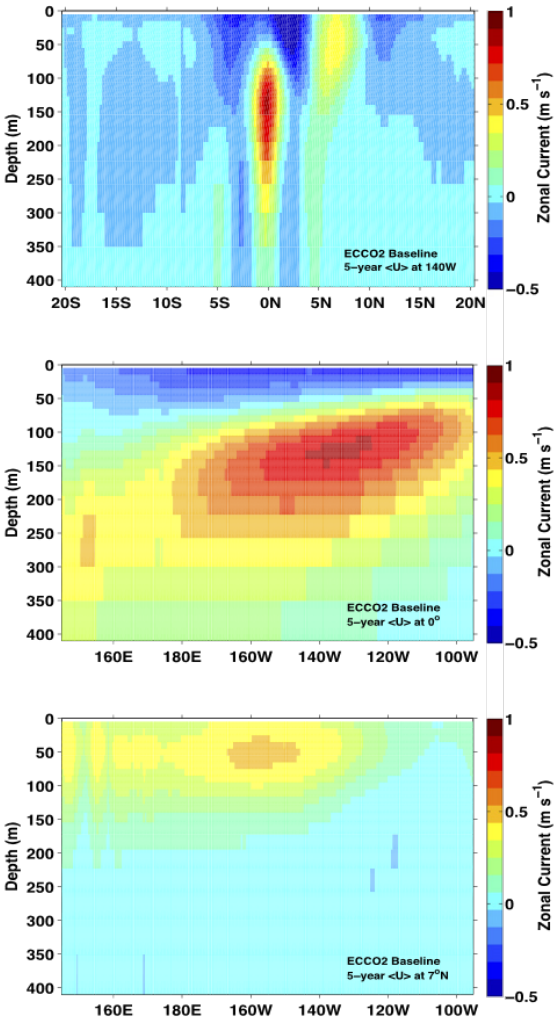

FIG. 3. ECCO2 Baseline 3-day zonal current solutions averaged over 2004–05 and 2009–11 for the upper 400 m: (a) 20°S–20°N along 140°W, (b) along the equator from 145°E to 95°W, and (c) along 7°N from 145°E to 95°W.

distribution of zonal currents along 140°W was computed for the ECCO2 Baseline solutions. The eastward-flowing EUC and NECC appear prominently above 400-m depth at the equator and near 7°N, respectively (Fig. 3a); the vertical dimensions and maximum values of the two currents agreed very well with shipboard ADCP measurements recorded over many years (Johnson et al. 2001). Figure 3a is representative of the meridional distribution of the zonal current at longitudes between 145°E and 95°W, which is the region where both currents are unperturbed by land. Also, the generation regions of the EUC and NECC occur west of 145°E, where the circulation is complex with interleaving currents and permanent eddies (Tozuka et al. 2002; Qu et al. 1999). The depth of the EUC core speed decreased from 225 m at 145°E to 75 m at 95°W and the maximum EUC core speed occurred at about 135°W at approximately 125 m (Fig. 3b); both features were in excellent agreement with multiyear shipboard ADCP observations reported by Johnson et al. (2001). The 5-yr-averaged maximum NECC speed occurred at about 150°W and 50-m depth (Fig. 3c).

The eastward volume transport [hereinafter called transport with a unit of Sverdrup (Sv), where 1 Sv $\equiv 10^6\,\mathrm{m^3\,s^{-1}}$] was equal to $\int\int u(>0)\,dz\,dy$, where $u(>0)$ was the eastward component of the zonal current and dy and dz represented north–south and vertical distances, respectively. No westward flow was considered in the dy and dz intervals. Volume transports were computed between 1.5°S–1.5°N and 4°–10°N (Fig. 3a). The eastward flow for both currents occurred above 400 m (Fig. 3a).

The 5-yr mean EUC and NECC transports portrayed in Fig. 3a were 36.9 and 25.8 Sv, respectively; the corresponding Optimized EUC and NECC transports were 38.0 and 23.4 Sv, respectively. The differences between the Baseline and Optimized solutions were relatively small in 5-yr mean values at 140°W but, as will be described below, larger differences occurred over annual and smaller time intervals, which, presumably, captured a smaller number of episodic events like Kelvin waves and tropical instability waves.

A Baseline and Optimized EUC (NECC) transport difference greater than 5.5 (5.0) Sv was considered to be substantial because this threshold would have corresponded to a $5\,\mathrm{cm\,s^{-1}}$ current speed uncertainty had moored current meter measurements been taken over a 2.5° (3°) latitude-wide and 200-m-thick (150 m) EUC (NECC). Johnson et al. (2001) had reported $5\,\mathrm{cm\,s^{-1}}$ accuracy for shipboard ADCP measurements. The t test was used to evaluate the 95% statistical significance when annual-mean values of the 3-day Baseline and Optimized EUC (NECC) transport differences were above 5.5 (5.0) Sv. Data assimilation is defined to have an impact on annual-mean values when the Baseline and Optimized EUC (NECC) transport difference was greater than 5.5 (5.0) Sv and the t test indicated the mean difference was statistically significant with 95% confidence.

c. *Equatorial Undercurrent*

For the annual-mean EUC transport, data assimilation had an impact but not always and not everywhere. The ECCO2 Baseline and Optimized EUC transports were equivalent at all longitudes in 2004, 2005, and 2009 but were significantly different in 2010 and 2011 over a large range of longitudes in the western and central Pacific (Fig. 4), where Optimized transports were larger than Baseline transports by about 10 Sv or 25%–35%.

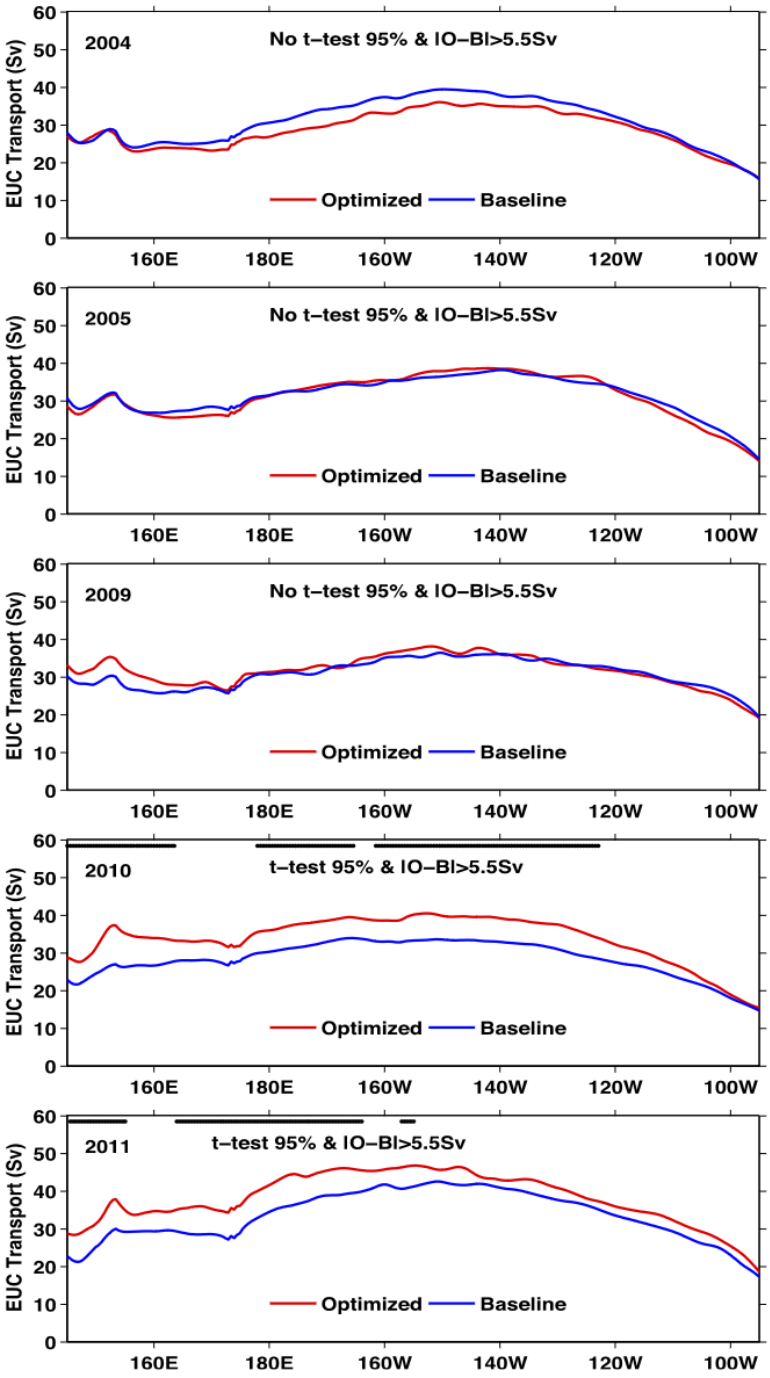

FIG. 4. ECCO2 Baseline and Optimized annual-mean EUC transports from 145°E to 95°W for each year for 2004–05 and 2009–11. The year is shown in the top-left corner of each panel. Baseline and Optimized solutions are indicated by blue and red curves, respectively. Black dots are displayed at the top portion of each panel at longitudes where annual-mean values of ECCO2 Baseline and Optimized 3-day solutions were statistically different with 95% confidence according to the *t*-test technique and also where the annual-mean difference was greater than 5.5 Sv.

The EUC is driven by the easterly surface wind stress in the equatorial waveguide (McCreary 1976). Different sources of surface winds in 2004–05 and 2009–11 (Table 1) may explain, to some extent, the different impacts in 2004–05 compared to 2009–11. Perhaps the intense La Niña from July 2010 to March 2011 had an influence. However, the difference between the results in 2010–11 and that in 2009 could not be attributed to different surface atmospheric datasets because the origin of the datasets was the same throughout 2009–11 and no substantial modifications were known to have occurred in the JMA methodology for the 2009 and 2010–11 datasets. The amount of in situ data assimilated within the 2°–3° latitude waveguide, which also is equivalent to the length of the first-mode Rossby radius of deformation (Chelton et al. 1998) and therefore the primary region of EUC dynamics, was considerably greater in 2005 compared to 2010 in the west and central regions (Fig. 1), illustrating the difficulty in separating the impacts caused by wind stress and assimilation of in situ salinity and temperature profile data. Salinity profiles, which would have an important impact on EUC dynamics (Behringer 2007), were not a major source of assimilated data in 2005 because the Argo program had not yet reached maturity. Baseline and Optimized EUC transport differences in 2010 and 2011 were approximately the same (Fig. 4), although the number of Argo temperature and salinity profiles acquired within the equatorial waveguide was much smaller in 2010 than in 2011 (Fig. 1), indicating the robust influence of assimilation of a smaller number of Argo temperature and salinity profiles.

Other studies with different methodologies, different datasets, and different time intervals have examined the impact of data assimilation on the vertical profile of zonal current at the equator. To compare our results with others, we visually determined the EUC transport per unit width from depth–longitude sections of zonal current along the equator and vertical profiles of zonal current published in the recent peer-reviewed literature; only recent contributions were examined because technological advances in data assimilation are rapidly occurring. In the eastern Pacific—for example, 140° and 110°W—our result that data assimilation had no impact on the 5-yr mean EUC transport (Fig. 4) was not consistent with the results of Huddleston et al. (2004), Hoteit et al. (2010), Balmaseda et al. (2013) and Karspeck et al. (2013), which indicated that assimilation of data increased the EUC transport, and was not similar to the Hyder et al. (2012) result that data assimilation reduced the EUC transport at 140°W. In the western Pacific—for example, 165°E and 170°W—we found data assimilation to have no impact in some years and it increased EUC transport in other years. Huddleston et al. (2004), Hoteit et al. (2010), and Balmaseda et al. (2013) reported that data assimilation increased the EUC transport in the western Pacific, but Karspeck et al. (2013) found that data assimilation reduced the EUC transport. Hoteit et al. (2010 assimilated NOAA in situ moored current measurements recorded along the equator, unlike other studies.

Comparison of results determined with different OGCMs and surface winds, which would yield different Baseline solutions, and with different datasets for assimilation and different data assimilation schemes over different averaging periods from months to years is an intellectual curiosity. It is tempting to speculate that the small impact on the EUC transport of adjoint method optimization for ECCO2 solution is caused by careful prior adjustment of model parameters. In particular, the vertical diffusivity was adjusted using a Green's function approach, leading to a much more realistic representation of equatorial stratification (e.g., Fig. 14, left column in Menemenlis et al. 2005) prior to adjoint method optimization.

d. North Equatorial Countercurrent

We did not know a priori whether the NECC transport would increase, decrease, or remain unchanged with data assimilation. Figure 5 shows the annual-mean NECC Baseline and Optimized transports in 2004–05 and 2009–11. In 2004 the impact of data assimilation was negligible at all longitudes except for a small region west of 160°E. This virtual absence of impact of data assimilation stands in marked contrast to the other four years. In 2005 data assimilation significantly reduced the NECC transport by about 10 Sv (or about 50%) over a large region from 175°E to 125°W. In 2009, data assimilation reduced the NECC transport by 10 Sv (or 35%) west of 170°W. In 2010 and 2011 the amount of the decrease was about 20 Sv (or 50%) west of 140°W, except west of 160°E in 2011 when the reduction approached 30 Sv (or 250%) at 145°E.

The time dependence of annual-mean values could have been caused by the relative scarcity of Argo data in the 4°–10°N region in 2004 compared to other years (Fig. 1). The ocean data assimilation impact region from 175°E to 125°W in 2005 was consistent with this speculation because this region coincided with plentiful Argo data. The increase in the quantity of Argo data in 2009–11 in the NECC region mirrored the intensity of the impact of data assimilation with the maximum reduction in the NECC transport (>30 Sv or 250%) in 2011 at 145°E (Fig. 5). It was not surprising that the NECC would respond dramatically to the assimilation of temperature and salinity profile measurements because the NECC is, to first order, in geostrophic balance. The influence of

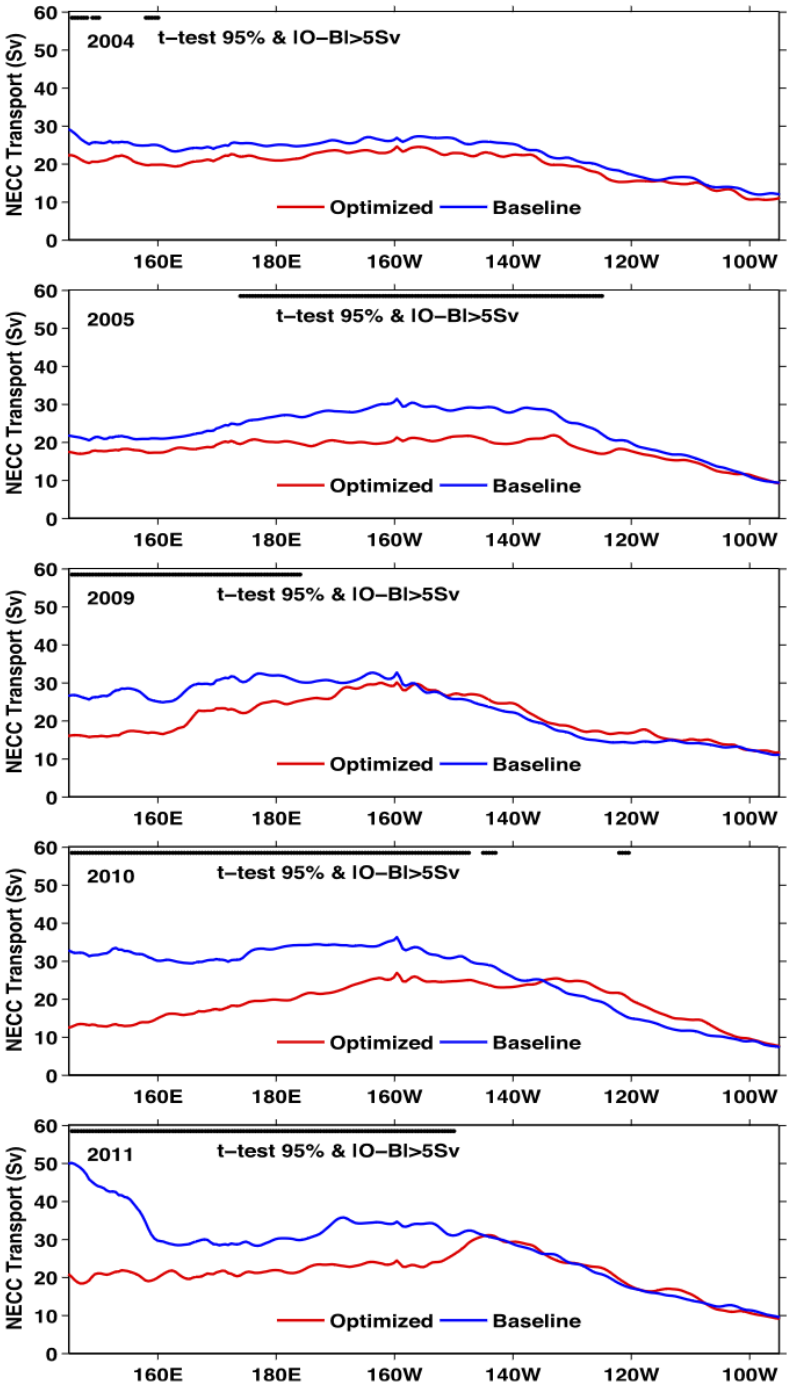

FIG. 5. As in Fig. 4, but for NECC transports where the annual-mean difference was greater than 5 Sv.

Ekman pumping and suction through the surface wind stress curl, which had the same data generation source in 2004–05 but different in 2009–11 (Table 1), may also have contributed to the annual impact of data assimilation.

Observations of space–time variations of the NECC transport are meager. Yu et al. (2000), through analyses of XBT measurements, indicated that the NECC mean transport monotonically decreased from 145°E to 110°W with a slope of ~5:1. The combined 5-yr mean Optimized solution inferred from Fig. 5 portrayed a different longitudinal profile, which had maximum transport (23 Sv) in the central Pacific at about 160°W, a smaller value (18 Sv) at 145°E, and a much smaller transport (10 Sv) at 95°W.

The El Niño/La Niña phenomenon was expected to impact interannual variations of the NECC transport because the north–south gradient of sea level, surface wind stress, and surface wind stress curl, with its impact on thermocline depth, would be different in the 4°–10°N region during El Niño and La Niña. Kashino et al. (2009), through analysis of shipboard ADCP observations, reported the NECC transport at 130°E was larger during El Niño than La Niña. The ECCO2 results were different than those by Kashino et al. (2009). ECCO2 Optimized NECC transports at 145°E ranged from 12 to 22 Sv in 2004, 2005, 2009, and 2010 (Fig. 5), which are considered to be normal years when each annual-mean oceanic Niño index (ONI) (http://www.cpc.ncep.noaa.gov/products/analysis_monitoring/ensostuff/ensoyears.shtml) was less than |0.5|. In 2011, a La Niña year with an ONI of −0.7, the Optimized transport at 145°E was ~20 Sv, which was within the range associated with a normal year. Chiswell et al. (1995) noted, through analysis of shipboard ADCP measurements at about 160°W, that the NECC transport was 3 times larger during La Niña conditions compared to El Niño conditions. In contrast to the observed El Niño/La Niña pattern at 160°W, the ECCO2 Optimized NECC transport at 160°W ranged from 18 to 28 Sv during normal years and was 20 Sv in the La Niña year. The Chiswell et al. (1995) and Kashino et al. (2009) observations on the influence of El Niño/La Niña on the NECC transport do not agree with each other and also do not agree with the Optimized solutions, which showed no difference between normal years and a La Niña year.

Note that the Chiswell et al. (1995) and Kashino et al. (2009) NECC transport observations were made over 3 or 4 days when ubiquitous intraseasonal fluctuations superimposed on a strong annual cycle would degrade the interpretation of limited-duration data. Intraseasonal fluctuations with substantial amplitudes were captured by Optimized and Baseline solutions at 170°, 140°, and 110°W (Fig. 6). Data assimilation greatly increased the amplitude of the fluctuations in 2005 and 2011, when the Optimized fluctuations were twice as large as the corresponding Baseline fluctuations.

Time series of the NECC transports were produced at longitudes arbitrarily chosen to coincide with the longitudes of the moored buoys along the equator where the EUC transports were discussed above. Beginning in 2009, the differences between the Baseline and Optimized NECC transports at 147°E were substantially larger compared to that in 2004–05 (Fig. 6) and where the Baseline and Optimized NECC transport differences increased steadily with time, reaching more than 35 Sv in June–September 2011. Apparently, data assimilation adjusted ECCO2 solutions toward values similar to those in previous years.

Assimilation of data produced a virtual disappearance of the NECC at 147° and 165°E in July–August 2010 and again in July–August 2011, when Baseline NECC transports were 15 and 35 Sv, respectively (Fig. 6). The Optimized solutions at 147° and 165°E captured the near-zero minimum NECC transport in all 5 years, but the Baseline solutions captured this feature only in 2004–05. In 2009 and 2010, the annual minimum Baseline NECC transports were considerably larger compared to 2004–05 and in 2011 the minimum transport had grown to approximately the same size as the annual maximum transports in the previous 4 years (Fig. 6). As in the case of the EUC, different sources of surface winds in 2004–05 and 2009–11 (Table 1) may explain, to some extent, the different impacts in 2004–05 compared to 2009–11. Apparently, assimilation of Argo temperature and salinity profiles constrained the Optimized solution to reproduce the essential features of the annual cycle in 2009–11, which were comparable to those in 2004–05, especially the annual interval of several months of low transport. An annual cycle of the NECC transport was expected because the surface wind stress curl (Risien and Chelton 2008), which influences the north–south gradient of the thermocline and, consequently, eastward geostrophic flow, has an annual cycle, especially east of 150°W, where a weak (strong) NECC would be expected to occur in April (October). Wyrtki (1965) captured this feature in surface current analysis in the eastern Pacific, and so did the ECCO2 Optimized and Baseline solutions at 140° and 110°W in 2004, 2005, and 2009 (Fig. 6). Lolk (1992), in an OGCM simulation without data assimilation of the climatological-mean annual cycle of the NECC from 150°E to 110°W, reported minimum and maximum NECC transports in March and September, respectively.

In the western Pacific at 165°E, the annual minimum (maximum) NECC transport occurred about 3 months later compared to the eastern Pacific, for example, in July–August (December–January) (Fig. 6). Perhaps the annual NECC transport cycle established in the eastern

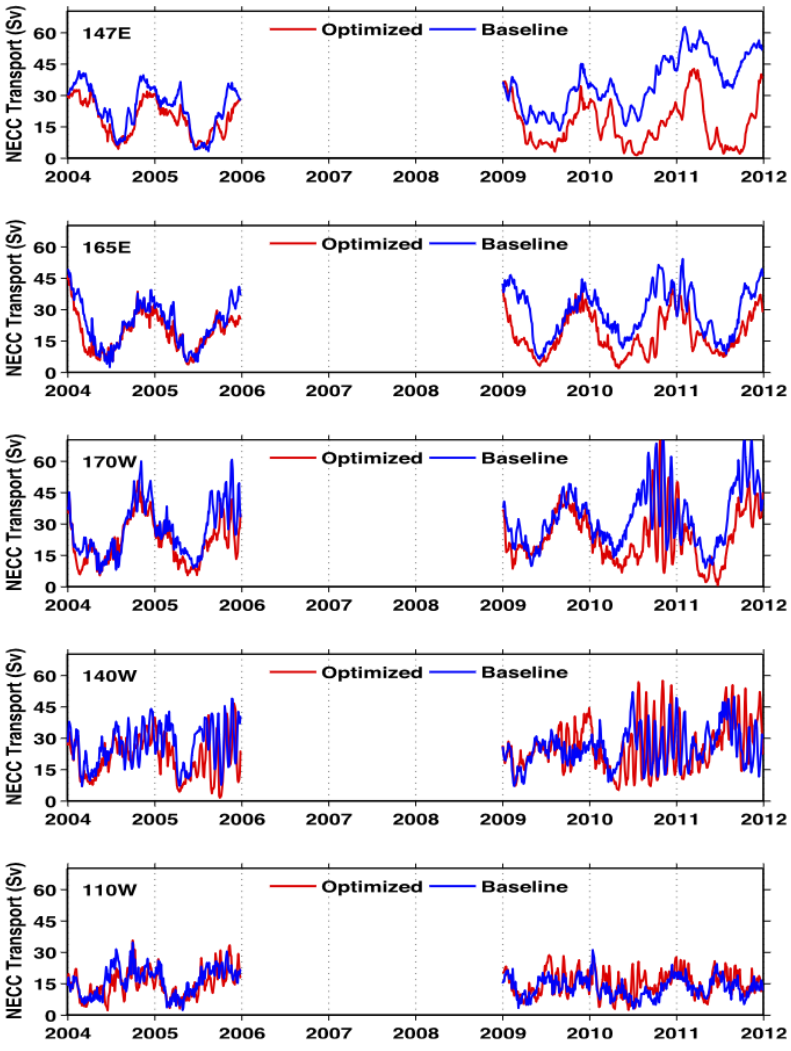

FIG. 6. Time series of ECCO2 Baseline and Optimized 3-day-averaged NECC transports at five longitudes along the Pacific equator. Longitudes are shown in the top-left corner of each panel. Baseline and Optimized solutions are indicated by blue and red curves, respectively.

Pacific propagated westward as an annual Rossby wave (Mitchum and Lukas 1990).

4. Concluding remarks

The ECCO2 Optimized EUC transports per unit width at 0°, 140°W and 0°, 110°W had similar features as those calculated with in situ ADCP observations. This correspondence provided opportunities to use ECCO2 Baseline and Optimized solutions to describe the impact of data assimilation on the EUC and NECC transports from 145°E to 95°W over 2004–05 and 2009–11. Space and time intervals occurred when data assimilation had no impact and other intervals when data assimilation greatly impacted the transports. When data assimilation had an impact, it increased the EUC transport and decreased the NECC transport, and the magnitude of the impact was far greater for the NECC than the EUC. For the NECC, we provide here the first description of the space–time structure of the impact of data assimilation. For the EUC, no simple summary of our results and those of others (e.g., Karspeck et al. 2013; Balmaseda et al. 2013; Hyder et al. 2012; Behringer 2007; Bell et al. 2004; Huddleston et al. 2004) on the impact of data assimilation is conclusive. A round-robin experiment is warranted to compare the impact of data assimilation on the EUC transport, in

which a consistent Baseline solution and methodology are compared.

The EUC and NECC are dependent on the surface wind stress and surface wind stress curl, respectively. Our numerical experiment, which was not designed to unravel the relative importance of individual datasets, used atmospheric surface variables from different sources in 2004–05 and 2009–11. Also, TAO temperature profiles were not assimilated.

Additional studies are warranted to determine the impact of assimilating different datasets on the EUC and NECC. Topics for additional study are the cause and dynamical balance of the annual occurrence of near-zero NECC transport throughout the width of the Pacific, and NECC response to El Niño and La Niña. The 21-yr record-length ECCO Central Production, version 4 (G. Forget et al. 2014, unpublished manuscript), which was released in February 2014, could be used for such analyses.

Acknowledgments. We appreciate the helpful suggestions on a draft manuscript by Dr. David Behringer (NOAA), and the perceptive comments and suggestions by three anonymous reviewers greatly improved the manuscript. We gratefully acknowledge support from Drs. David Considine and Jack Kaye (both at NASA headquarters). Hong Zhang kindly made Fig. 1. The research was carried out in part at the Jet Propulsion Laboratory, California Institute of Technology, under a contract with NASA.

REFERENCES

Balmaseda, M. A., K. Mogensen, and A. T. Weaver, 2013: Evaluation of the ECMWF ocean reanalysis system ORAS4. *Quart. J. Roy. Meteor. Soc.,* **139,** 1132–1161, doi:10.1002/qj.2063.

Behringer, D. W., 2007: The Global Ocean Data Assimilation System (GODAS) at NCEP. *11th Symp. on Integrated Observing and Assimilation Systems for the Atmosphere, Oceans, and Land Surface,* San Antonio, TX, Amer. Meteor. Soc., 3.3. [Available online at https://ams.confex.com/ams/87ANNUAL/techprogram/paper_119541.htm.]

Bell, M. J., M. J. Martin, and N. K. Nichols, 2004: Assimilation of data into an ocean model with systematic errors near the equator. *Quart. J. Roy. Meteor. Soc.,* **130,** 873–893, doi:10.1256/qj.02.109.

Bindoff, N. L., and Coauthors, 2007: Observations: Oceanic climate change and sea level. *Climate Change 2007: The Physical Science Basis,* S. Solomon et al., Eds., Cambridge University Press, 385–432.

Carton, J. A., G. Chepurin, X. Cao, and B. Giese, 2000: A Simple Ocean Data Assimilation analysis of the global upper ocean 1950–95. Part I: Methodology. *J. Phys. Oceanogr.,* **30,** 294–309, doi:10.1175/1520-0485(2000)030<0294:ASODAA>2.0.CO;2.

Chelton, D. B., R. A. deSzoeke, M. G. Schlax, K. El Naggar, and N. Siwertz, 1998: Geographical variability of the first baroclinic Rossby Radius of deformation. *J. Phys. Oceanogr.,* **28,** 433–460, doi:10.1175/1520-0485(1998)028<0433:GVOTFB>2.0.CO;2.

Chiswell, S. M., K. A. Donohue, and M. Wimbush, 1995: Variability in the central equatorial Pacific, 1985–1989. *J. Geophys. Res.,* **100,** 15 849–15 863, doi:10.1029/95JC01379.

Forget, G., 2010: Mapping ocean observations in a dynamical framework: A 2004–06 ocean atlas. *J. Phys. Oceanogr.,* **40,** 1201–1221, doi:10.1175/2009JPO4043.1.

——, and C. Wunsch, 2007: Global hydrographic variability and the data weights in oceanic state estimates. *J. Phys. Oceanogr.,* **37,** 1997–2008, doi:10.1175/JPO3072.1.

Hallberg, R., 2013: Using a resolution function to regulate parameterizations of oceanic mesoscale eddy effects. *Ocean Modell.,* **72,** 92–103, doi:10.1016/j.ocemod.2013.08.007.

Halpern, D., I. Fukumori, D. Menemenlis, and X. Wang, 2013: Long range Kelvin wave propagation of transport variations in the Pacific Ocean equatorial currents: Part II. *2013 Fall Meeting,* San Francisco, CA, Amer. Geophys. Union, Abstract OS32A-03.

Hoteit, I., B. Cornuelle, and P. Heimbach, 2010: An eddy-permitting, dynamically consistent adjoint-based assimilation system for the tropical Pacific: Hindcast experiments in 2000. *J. Geophys. Res.,* **115,** C03001, doi:10.1029/2009JC005437.

Huddleston, M. R., M. J. Bell, M. J. Martin, and N. K. Nichols, 2004: Assessment of wind-stress errors using bias corrected ocean data assimilation. *Quart. J. Roy. Meteor. Soc.,* **130,** 853–871, doi:10.1256/qj.02.213.

Hyder, P., D. Storkey, E. Blackley, C. Guiavarc'h, J. Siddorn, M. Martin, and D. Lea, 2012: Assessing equatorial surface currents in the FOAM global and Indian Ocean models against observations from the global tropical moored array. *J. Oper. Oceanogr.,* **5,** 25–39.

Johnson, G. C., M. J. McPhaden, and E. Firing, 2001: Equatorial Pacific Ocean horizontal velocity, divergence, and upwelling. *J. Phys. Oceanogr.,* **31,** 839–849, doi:10.1175/1520-0485(2001)031<0839:EPOHVD>2.0.CO;2.

Karspeck, A. R., S. Yeager, G. Danabasoglu, T. Hoar, N. Collins, K. Raeder, J. Anderson, and J. Tribbia, 2013: An ensemble adjustment Kalman filter for the CCSM4 ocean component. *J. Climate,* **26,** 7392–7413, doi:10.1175/JCLI-D-12-00402.1.

Kashino, Y., N. Espana, F. Syamsudin, K. J. Richards, T. Jensen, P. Dutrieux, and A. Ishida, 2009: Observations of the North Equatorial Current, Mindanao Current, and Kuroshio current system during the 2006/07 El Niño and 2007/08 La Niña. *J. Oceanogr.,* **65,** 325–333, doi:10.1007/s10872-009-0030-z.

Knox, R. A., and D. Halpern, 1982: Long range Kelvin wave propagation of transport variations in Pacific Ocean equatorial currents. *J. Mar. Res.,* **40** (Suppl.), 329–339.

Large, W. G., J. C. McWilliams, and S. Doney, 1994: Oceanic vertical mixing: A review and a model with a nonlocal boundary-layer parameterization. *Rev. Geophys.,* **32,** 363–403, doi:10.1029/94RG01872.

Lolk, N. K., 1992: Annual and longitudinal variations of the Pacific North Equatorial Countercurrent. Jet Propulsion Laboratory Tech. Rep. JPL-PUBL-92-8, 221 pp.

Martin, J. H., and Coauthors, 1994: Testing the iron hypothesis in ecosystems of the equatorial Pacific Ocean. *Nature,* **371,** 123–129, doi:10.1038/371123a0.

McCreary, J., 1976: Eastern tropical ocean response to changing wind systems: With application to El Niño. *J. Phys. Oceanogr.,* **6,** 632–645, doi:10.1175/1520-0485(1976)006<0632:ETORTC>2.0.CO;2.

McPhaden, M. J., and Coauthors, 1998: The Tropical Ocean Global Atmosphere (TOGA) observing system: A decade of

progress. *J. Geophys. Res.,* **103,** 14 169–14 240, doi:10.1029/97JC02906.

Menemenlis, D., I. Fukumori, and T. Lee, 2005: Using Green's functions to calibrate an ocean general circulation model. *Mon. Wea. Rev.,* **133,** 1224–1240, doi:10.1175/MWR2912.1.

——, J.-M. Campin, P. Heimbach, C. Hill, T. Lee, A. Nguyen, M. Schodlok, and H. Zhang, 2008: ECCO2: High resolution global ocean and sea ice data synthesis. *Mercator Ocean Quarterly Newsletter,* No. 31, Mercator Ocean, Ramonville Saint-Agne, France, 13–21.

Mitchum, G. T., and R. Lukas, 1990: Westward propagation of annual sea level and wind signals in the western Pacific Ocean. *J. Climate,* **3,** 1102–1110, doi:10.1175/1520-0442(1990)003<1102:WPOASL>2.0.CO;2.

Philander, S. G., 1990: *El Niño, La Niña, and the Southern Oscillation*. International Geophysics Series, Vol. 46, Academic Press, 293 pp.

Qu, T., H. Mitsudera, and T. Yamagata, 1999: A climatology of the circulation and water mass distribution near the Philippine coast. *J. Phys. Oceanogr.,* **29,** 1488–1505, doi:10.1175/1520-0485(1999)029<1488:ACOTCA>2.0.CO;2.

Risien, C. M., and D. B. Chelton, 2008: A global climatology of surface wind and wind stress fields from eight years of QuikSCAT scatterometer data. *J. Phys. Oceanogr.,* **38,** 2379–2413, doi:10.1175/2008JPO3881.1.

Takahashi, T., and Coauthors, 2009: Climatological mean and decadal change in surface ocean pCO_2, and net sea–air flux over the global oceans. *Deep-Sea Res. II,* **56,** 554–577, doi:10.1016/j.dsr2.2008.12.009.

Tollefson, J., 2014: El Niño monitoring system in failure mode. *Nature,* doi:10.1038/nature.2014.14582.

Tozuka, T., T. Kagimoto, Y. Masumoto, and T. Yamagata, 2002: Simulated multiscale variations in the western tropical Pacific: The Mindanao Dome revisited. *J. Phys. Oceanogr.,* **32,** 1338–1359, doi:10.1175/1520-0485(2002)032<1338:SMVITW>2.0.CO;2.

Vernieres, G., M. M. Rienecker, R. Kovach, and C. L. Keppenne, 2012: The GEOS-iODAS: Description and evaluation. Technical Report Series on Global Modeling and Data Assimilation, Vol. 30, NASA Tech. Memo. NASA/TM-2012-104606, 61 pp.

Wunsch, C., and P. Heimbach, 2007: Practical global ocean state estimation. *Physica D,* **230,** 197–208, doi:10.1016/j.physd.2006.09.040.

——, ——, R. M. Ponte, I. Fukumori, and the ECCO-GODAE Consortium Members, 2009: The global general circulation of the ocean estimated by the ECCO-Consortium. *Oceanography,* **22,** 88–103, doi:10.5670/oceanog.2009.41.

Wyrtki, K., 1965: Surface currents of the eastern tropical Pacific Ocean. *Bull. - Inter-Amer. Trop. Tuna Comm.,* **9,** 271–304.

——, and B. Kilonsky, 1984: Mean water and current structure during the Hawaii-to-Tahiti Shuttle Experiment. *J. Phys. Oceanogr.,* **14,** 242–254, doi:10.1175/1520-0485(1984)014<0242:MWACSD>2.0.CO;2.

Yu, Z., J. P. McCreary Jr., W. S. Kessler, and K. A. Kelly, 2000: Influence of equatorial dynamics on the Pacific North Equatorial Countercurrent. *J. Phys. Oceanogr.,* **30,** 3179–3190, doi:10.1175/1520-0485(2000)030<3179:IOEDOT>2.0.CO;2.